Journal of Magnetic Resonance **136,** 159–168 (1999)
Article ID jmre.1998.1612, available online at http://www.idealibrary.com on IDEAL®

SPRITE MRI with Prepared Magnetization and Centric *k*-Space Sampling

Igor V. Mastikhin, Bruce J. Balcom,[1] Pablo J. Prado, and Christopher B. Kennedy

MRI Centre, Department of Physics, P.O. Box 4400, University of New Brunswick, Fredericton, New Brunswick, E3B 5A3, Canada

E-mail bjb@unb.ca

Received April 6, 1998; revised September 22, 1998

A technique for imaging materials with short transverse relaxation times and prepared longitudinal magnetization is proposed. The technique is single-point ramped imaging with T_1-enhancement (SPRITE) MRI with centric *k*-space sampling. The effects of transient state behavior on image resolution and signal/noise are estimated. Centric sampling in the basic SPRITE sequence gives increased signal-to-noise and permits a quantitative determination of the MR parameters associated with longitudinal spin preparation. Spin-lock and inversion recovery preparation experiments are presented.

INTRODUCTION

Single-point imaging (SPI) methods (Fig. 1a) have proven their worth for studies of short relaxation time systems (*1*, *2*). Gravina and Cory (*3*) have discussed the sensitivity and resolution characteristics of SPI, which is also termed constant time imaging. SPI methods assume that the RF pulse bandwidth is sufficient to ensure homogeneous excitation of the sample at all gradient values. The RF pulses are applied in the presence of phase encode gradients, the phase encode time t_p is constant, and only one point of *k*-space is sampled for each excitation pulse. Switching gradients on and off for each *k*-space point is inefficient, yet the absence of RF slice selection makes the method intrinsically three-dimensional and thereby requires pulsed gradients in all three dimensions. As a pure phase encoding method, distortions due to magnetic susceptibility, chemical shift, and other unwanted time-evolution effects are eliminated. Sharp *et al.* (*4*) have discussed the same advantages, which accrue from sampling single points from multiple echoes, individually phase encoded.

Our modification of SPI, single-point ramped imaging with T_1-enhancement (SPRITE) (*5*), consists of a ramped phase encode gradient in the primary phase encode direction and conventional phase encode gradients in the other (secondary) directions (Fig. 1b). The use of a ramped phase gradient permits imaging with greater speed and with lower dB/dt, which minimizes gradient vibration. A great time improvement is achieved with samples where T_1 relaxation times are on the order of the gradient rise time (*6*, *7*).

The SPRITE technique also works well for samples with longer T_1-relaxation times, such as polymers and elastomers (*8*), where one can manipulate image contrast through partial saturation of longitudinal magnetization. Steady-state longitudinal magnetization yields an observed magnetization, M_y, which is given by Eq. [1] (*9*),

$$M_y = M_0 \frac{1 - E}{1 - CE} \sin \alpha \qquad [1]$$

where $E = \exp(-\mathrm{TR}/T_1)$ and C is the cosine of flip angle α.

For solid-like samples, a vast array of preparation techniques (inversion, spin echo, solid echo, dipolar echo, spin-locking magnetization filters) can be employed to deduce molecular information, spatially resolved through MRI (*10*). Magnetization preparation is easily incorporated into the SPI-sequence by sampling a single k-space point after each magnetization filter application. Beyea *et al.* have demonstrated (*6*) that magnetization preparation permits accurate T_2- and T_1-mapping of samples with short relaxation times. The necessity of waiting for T_1-recovery after each sampled point makes this method very time-consuming for materials with long T_1's. It seems very natural therefore to utilize longitudinal magnetization more efficiently and sample, with SPRITE, a whole line of *k*-space for each magnetization filter application.

In the general case, as longitudinal magnetization evolves during sampling, our SPRITE technique will be a "transient-state" imaging method (*11*). The dynamic approach to steady state may cause relaxation blurring and transverse magnetization oscillations (*12*, *13*) in conventional transient-state spin warp imaging. With short T_2^* samples, combined with active gradient spoiling when necessary (*8*), unwanted and deleterious transverse magnetization is eliminated with the SPRITE technique.

In this paper we outline the use of centric order sampling,

[1] To whom correspondence should be addressed.

1090-7807/99 $30.00

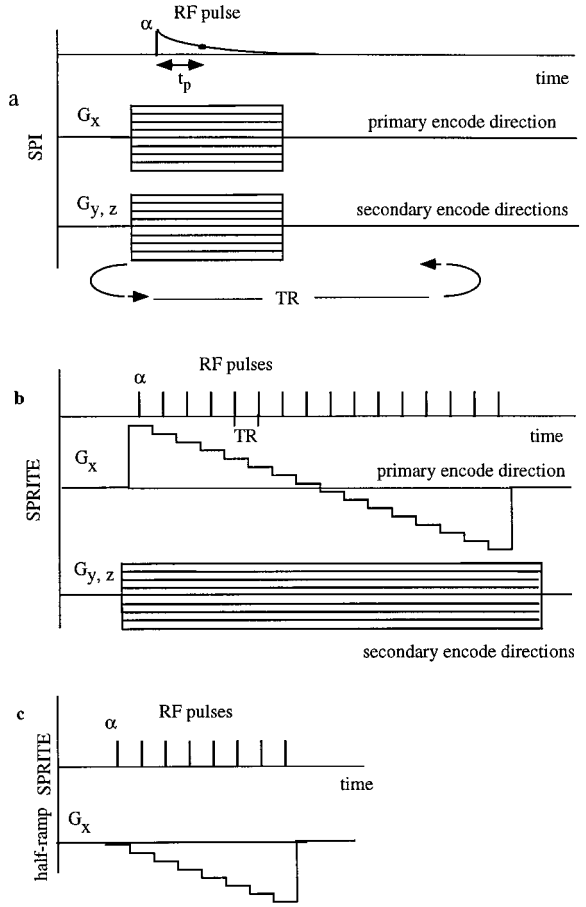

FIG. 1. (a) Single point imaging (SPI) sequence. The image is phase encoded with amplitude cycling of the gradient along the imaging axis. A single point is acquired after phase encode time t_p following an RF pulse with flip angle α. The repetition time is TR. (b) SPRITE imaging sequence. The gradient is stepped with an RF pulse at every gradient level. Typically, 64 steps are employed, each of approximately 0.5–4.5 ms duration. As in (a), a single complex point is acquired following each RF pulse. The encoding time is t_p and the repetition time is TR. (c) Half-ramp SPRITE sequence, with acquisition in the primary encode direction beginning at the *k*-space origin.

half-*k*-space acquisition, and prepared magnetization with the SPRITE technique. We discuss how these ideas influence image resolution, amplify sensitivity to magnetization preparation, increase signal/noise, and reduce the total acquisition time.

THEORY

Finite Sampling Effects on Image Resolution

Image space is related to reciprocal space through a Fourier transform operation on a sampled signal which may be evolving (longitudinal magnetization) as it is acquired.

$$M(x, y) = F\{M(k_x, k_y)U(t)R(t)\}$$

The operation F indicates the Fourier transform while $U(t)$ is the sampling function. The Fourier transform of $U(t)$ is the sampling point spread function (SPSF) and represents the effect of a finite sampling time. $M(k_x, k_y)$ is the sample magnetization in the absence of T_1 saturation effects. Note that T_2^* decay in SPI based methods will merely attenuate the signal $M(k_x, k_y)$. $R(t)$ is a relaxation function which controls T_1 contrast or T_1 blurring in the final image. After Fourier transformation the three functions are convolved:

$$M(x, y) = F\{M(k_x, k_y)\} \otimes F\{U(t)\} \otimes F\{R(t)\}.$$

When an image, matrix size N^2, is acquired with a field of view, FOV, and maximum phase encoding gradient value G_x,

$$\gamma G_x t_p \mathrm{FOV} = \pi N,$$

the nominal pixel resolution will be Δx, where t_p is the phase encoding time:

$$\Delta x = \frac{\mathrm{FOV}}{N} = \frac{\pi}{\gamma G_x t_p}.$$

The Fourier transform of $U(t)$ is a sinc function, which gives rise to image blurring (*14*). The SPSF pixel resolution is 21% more coarse than the nominal resolution:

$$\Delta x = \frac{1.2\pi}{\gamma G_x t_p}.$$

Relaxation Behavior of Signal during SPRITE

Digital filtering of the free induction decay (FID) is standard practice (*15*) in NMR as a postprocessing step to improve signal-to-noise (S/N), at the potential cost of decreased resolution. We show below that transient longitudinal magnetization, in a SPRITE acquisition, modulates the acquired signal in an exponential fashion and acts in a way entirely analogous to an exponential "filter" in conventional NMR.

For steady-state longitudinal M_z, all points of *k*-space are equally weighted with a known relaxation parameter, $R(t)$. Evolution to a longitudinal steady state during the image acquisition can be avoided by the application of dummy scans. More commonly, the longitudinal steady state is achieved at the periphery of *k*-space prior to the acquisition of significant signal intensity.

For the transient-state case, not all *k*-space points will have the same relaxation weightings. Two factors may influence this weighting: residual transverse magnetization and T_1-relaxation decay during the approach to steady state. Residual transverse magnetization, from previous RF pulses, may result in unwanted echoes (*16*) and consequent image artifacts. For systems with $T_2^* \sim 0.05$–1 ms, i.e., comparable to or much shorter than a single acquisition step (0.2–2 ms), residual

transverse magnetization is easily suppressed by "passive spoiling" (dephasing by phase encode gradients during acquisition steps) or "active spoiling" (dephasing by spoiler gradients).

If $\gamma\Delta G_x L_x$ TR $\ll 2\pi$ and $T_2^* \geq$ TR where ΔG_x is the primary phase gradient step used for encoding, and L_x is sample length in the x-direction, active spoiling is usually required. The spoiling gradient strength $G_{x,\text{spoil}}$ should fulfill

$$\gamma G_{x,\text{spoil}} L_x T_{\text{spoil}} \gg 2\pi,$$

where T_{spoil} is the spoiling time (*17*). As discussed by Kennedy *et al.* (*8*), active spoiling is required only during sampling around the k-space origin.

Since residual transverse magnetization and unwanted echoes are easily suppressed, we now consider M_z evolution during a SPRITE acquisition. M_i is the initial (prepared) Z-magnetization and M_0 is the equilibrium Z-magnetization. After the first RF pulse, M_z is equal to

$$M_{z1} = M_i CE + M_0(1 - E).$$

After the nth RF pulse, M_z is given by Eq. [2] (*13*):

$$M_{zn} = M_i C^n E^n + M_0(1 - E)\,\frac{1 - C^n E^n}{1 - CE}. \qquad [2]$$

Equation [2] may be rearranged, with $w = (1 - E)/(1 - CE)$, and the expression for Z-magnetization after the nth pulse, becomes Eq. [3]:

$$M_{zn} = (M_i - M_0 w)C^n E^n + M_0 w. \qquad [3]$$

The longitudinal magnetization and, consequently, the image intensity depend on two separate terms in Eq. [3]. The first term depends on n and is therefore the transient component. It influences image blurring. The second term, independent of n, is the steady-state component. It influences the image S/N. The extent of resolution blurring is therefore determined, not only by the T_1-relaxation time, but also by the ratio of transient-state and steady-state components. The parameter ϵ reflects the proportion of transient-state component in the observed signal:

$$\epsilon = \frac{(M_i - M_0 w)}{M_0 w} = \frac{M_i}{M_0 w} - 1.$$

Equation [3] may be rewritten, in terms of ϵ, with R_n the relaxation evolution function introduced in Eq. [1]:

$$M_{zn} = M_0(1 + \epsilon C^n E^n) = M_0 R_n$$

In the absence of magnetization preparation, $M_i = M_0$, $\epsilon = (1/w) - 1$, and therefore

$$M_{zn} = M_0(1 - w)C^n E^n + M_0 w.$$

The change in longitudinal magnetization with pulses, n, is known and therefore one can estimate the influence of M_z decay, during the acquisition, on resolution. We employ the notation of Vlaadingerbroek and den Boer (*11*) to represent $C^n E^n$ in terms of an apparent T_1:

$$C^n E^n = \exp\left(-\frac{nTR}{T_{\text{app}}}\right)$$

$$\frac{1}{T_{\text{app}}} = \left(\frac{1}{T_1} - \frac{\ln(\cos\alpha)}{\text{TR}}\right). \qquad [4]$$

Given that $k_x = \gamma\Delta G_x n t_p$, and hence $n = k_x/(\gamma\Delta G_x t_p)$, Fourier transformation of our new function for evolving longitudinal magnetization will produce a Lorentzian function:

$$F\left\{\exp\left(-\frac{k_x}{\gamma\Delta G_x T_{\text{app}}}\frac{\text{TR}}{t_p}\right)\right\} \rightarrow \frac{\gamma\Delta G_x T_{\text{app}}(\text{TR}/t_p)}{1 + i\gamma\Delta G_x T_{\text{app}}(\text{TR}/t_p)\,x}.$$

This function is the point spread function due to longitudinal spin evolution during sampling. We term it the "evolution point spread function" (EPSF). The linewidth is

$$\Delta x_{\text{EPSF}} = \frac{2}{\gamma\Delta G_x T_{\text{app}}}\frac{\text{TR}}{T_p}.$$

Recalling that $G_x = \Delta G_x N/2$ and comparing Δx_{SPSF} to Δx_{EPSF}, if our goal is to have evolution blurring smaller than that of the SPSF, $\Delta x_{\text{EPSF}}/\Delta x_{\text{SPSF}} < 1$:

$$\frac{\Delta x_{\text{EPSF}}}{\Delta x_{\text{SPSF}}} = \frac{N\text{TR}}{1.2\pi T_{\text{app}}} = \frac{N}{1.2\pi}\left(\frac{\text{TR}}{T_1} - \ln(\cos\alpha)\right).$$

The constraint of $\Delta x_{\text{EPSF}}/\Delta x_{\text{SPSF}} < 1$ places a limit on the k-space matrix size in the primary phase encode direction, for the no blurring case, once TR, T_1, and the flip angle are determined:

$$\frac{1}{N} > 0.26\left(\frac{\text{TR}}{T_1} - \ln(\cos\alpha)\right) \qquad [5]$$

Equation [5] permits one to estimate the limits where a dynamic approach to steady state begins to decrease resolution, by a comparison to the SPSF-limited resolution. Plots of the observed transverse magnetization for various flip angles and TR/T_1 ratios are shown in Fig. 2. For TR/T_1 = 0.01, 0.02, and 0.03 and for flip angle = 15°, ϵ is consequently 3.3, 4.8,

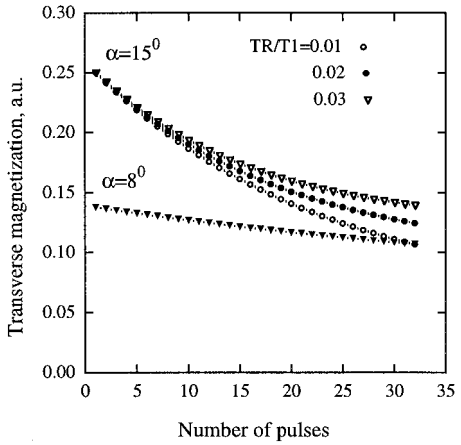

FIG. 2. Transient behavior of the observed magnetization during a pulse train, according to Eq. [3]. Note that for $TR/T_1 = 0.01$, the Ernst angle is $\alpha = 8°$ and the signal change is minimal.

and 5.9 and the transient-state component is more important than the steady-state component. Blurring caused by the transient component will dominate the resolution. For a flip angle of 15°, $\ln(\cos \alpha) = 0.034$, and from Eq. [5], if $TR = 0.01\ T_1$, the flip angle becomes the main "evolution parameter."

The choice of a large flip angle, to obtain more signal, will probably yield a resolution loss as illustrated in Fig. 3. For $\alpha = 15–20^0$ ($TR = 0.01\ T_1$, $N = 64$) a regime where resolution suffers has already been reached. An additional limitation on the use of large flip angles is the bandwidth restriction on the RF excitation. This limits our ability to vary the flip angle during an acquisition (*18*) to prevent M_z evolution which could otherwise decrease this "filter effect" on the image resolution.

Note that in the case of a half *k*-space acquisition, with the balance of *k*-space reconstructed by symmetry, the evolution curve will be symmetrical about the *k*-space origin. While the real part of the linewidth is the same as in the case of sampling from $-N/2$ to $N/2$, the imaginary part is equal to zero, and the magnitude linewidth is narrower.

Signal-to-Noise and Sensitivity to Magnetization Preparation

Since the image intensity will be principally determined by the low order *k*-space points, the sensitivity to prepared magnetization will be increased if sampling begins at the *k*-space origin.

If sampling is performed, beginning from high frequencies (full-ramp SPRITE), the *Z*-magnetization at the *k*-space zero is given by

$$M_{z(k=0)} = (M_i - M_0 w) C^{N/2} E^{N/2} + M_0 w. \qquad [6]$$

However, if centric sampling is performed, then $M_{z(k=0)}$ is simply the value of the prepared magnetization. This has two important consequences. (1) For conventional SPRITE encoding, the dependence of the image intensity on the prepared magnetization is much weaker than for centric order encoding. Conventional, full-ramp images will be greatly influenced by T_1-recovery as the system comes to equilibrium. (*2*) The image S/N is principally determined by the prepared magnetization for centric order encoding. For conventional, full-ramp encoding the image S/N is determined by the steady-state magnetization.

This suggests that one can improve both the sensitivity to any magnetization preparation technique and the image S/N using centric order SPRITE encoding. These ideas have previously been introduced in various modifications of spin-echo and gradient echo imaging (*19–23*), but none of these techniques permit the observation of short T_2^* solid-like samples.

As an example, with $TR/T_1 = 0.01$ and a 15° flip angle (Ernst angle would be 8°), the S/N for centric order encoding will be increased a factor of 3.7 in comparison to sequential order encoding with Ernst angle excitation. In principle, by varying the flip angle during sampling it is possible to increase signal while maintaining resolution (*24, 25*).

Secondary Phase Encode Directions

The primary phase encode direction is defined by the stepped ramp in Fig. 1a. The secondary phase encode gradients encode orthogonal directions. Let T_d be the time for magnetization recovery between successive *k*-space lines (ramps) in the primary phase direction. Longitudinal magnetization evolution effects in the secondary directions may occur if the delay time T_d is too short. Figure 4 shows how the simulated signal behaves, in a secondary dimension, for various delays after a ramped acquisition in the primary direction. If one assumes that M_z has entered a longitudinal steady state by the end of

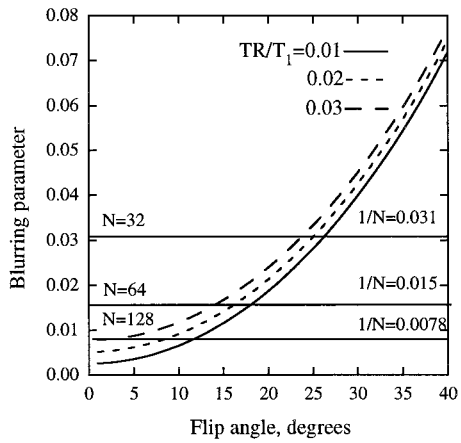

FIG. 3. Blurring vs flip angle, for $TR/T_1 = 0.01$, 0.02, and 0.03. Blurring is defined as the condition under which the EPSF becomes wider than SPSF. Here the blurring parameter is equal to $0.26[(TR/T_1) - \ln(\cos \alpha)]$. N is the number of points in the chosen dimension. Straight lines are plotted as references for various values of $1/N$. One can see that for $N = 64$ and flip angles exceeding 15°, blurring due to transient effects influences the image.

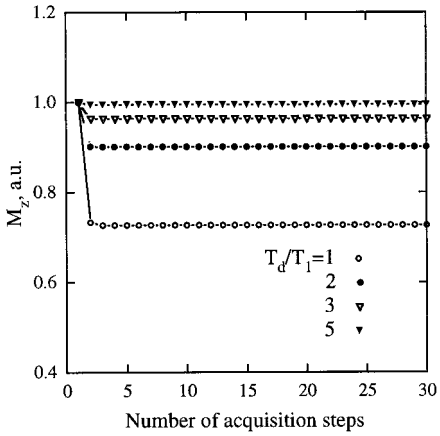

FIG. 4. Simulation of *Z*-magnetization approaching steady state in a secondary phase encoding direction for a (64 × 64) half *k*-space centric encoding experiment. T_d is the delay for magnetization recovery. The flip angle was 15°, TR/T_1 = 0.01.

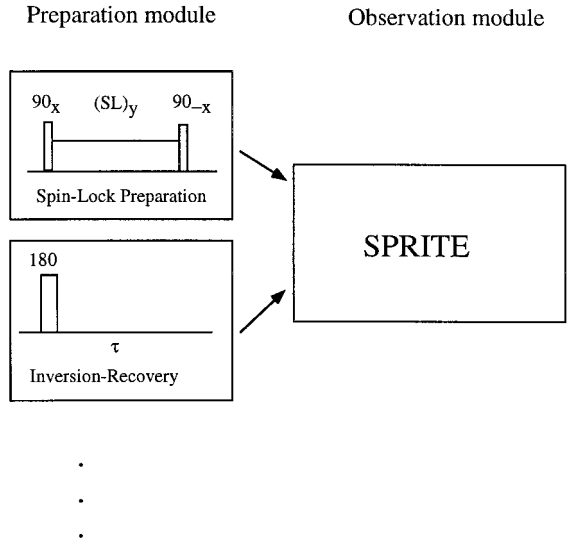

FIG. 5. SPRITE sequences used for imaging with prepared magnetization. The imaging module is constant (full or half *k*-space SPRITE) while the preparation part may vary. In this case we illustrate a spin lock *Z* storage preparation and an inversion recovery preparation. A large variety of preparation schemes are possible.

each primary phase encode *k*-space line, then for centric encoding a discontinuity occurs between the first and second *k*-space points in the secondary direction. This will influence the image *S*/*N* by altering the baseline but will not cause image blurring. For $T_d/T_1 = 2$ and centric encoding, M_z is close to its equilibrium value. The overall image acquisition is obviously faster in this case compared to $T_d/T_1 = 5$.

If *n*-fold signal averaging is required, the partial saturation effects on M_z in the secondary phase encode directions may require that the entire data matrix be acquired *n* times sequentially rather than the more conventional *n* repetitions of acquisitions of each individual line of *k*-space.

Half-k-space Acquisition

During a conventional SPRITE acquisition, phase encode gradients vary from $-G_x$ to G_x and one samples a full line of *k*-space during each magnetization cycle. Centric order encoding with the SPRITE-technique (half-ramp SPRITE) means that one collects data from only one half of *k*-space during each magnetization cycle. To collect the other half one must repeat the acquisition, and this is time-consuming. If magnitude images are desired, it is possible to exploit the inherent symmetry of *k*-space (*26*) to reconstruct the missing data. While extensively discussed in the literature, half *k*-space imaging is not very common in spin-warp imaging. The exact position of the center of the echo can be difficult to identify and inevitable phase errors occur. Numerous algorithms have been proposed to correct phase distortions in the final image (*27–29*). These methods usually require sampling somewhat more than half of *k*-space.

For SPI-based methods (especially applied to materials) we avoid these problems. Our *k*-space data is assembled point by point and we can exactly identify the zero-phase point. Susceptibility, magnetic field inhomogeneity, and other factors distorting phase in the case of spin-warp imaging lead only to attenuation of signal in SPI-based methods.

Half *k*-space acquisitions do have an inevitable *S*/*N* loss (exactly $\sqrt{2}$) because of fewer independent data points. However, centric order sampling is so advantageous that it can easily produce an *S*/*N* increase of more than a factor of 2. Reconsidering the previous example, a *S*/*N* gain of a factor of 3.7 due to centric sampling, even after the "half-k-space sampling loss," still has an *S*/*N* increase 2.6 times greater than for sequential sampling. A half *k*-space, centric ordered acquisition will also have much better preservation of the magnetization preparation in the final image.

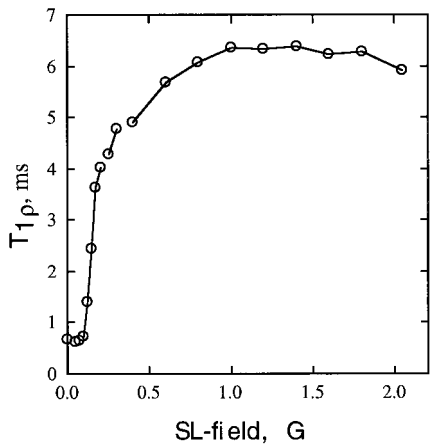

FIG. 6. Dependence of $T_{1\rho}$ on the applied spin-locking field for polyisoprene. It is seen that for SL fields less than 0.5 G, $T_{1\rho}$ is small. The SL field becomes comparable to local magnetic fields which determine the $T_{1\rho}$.

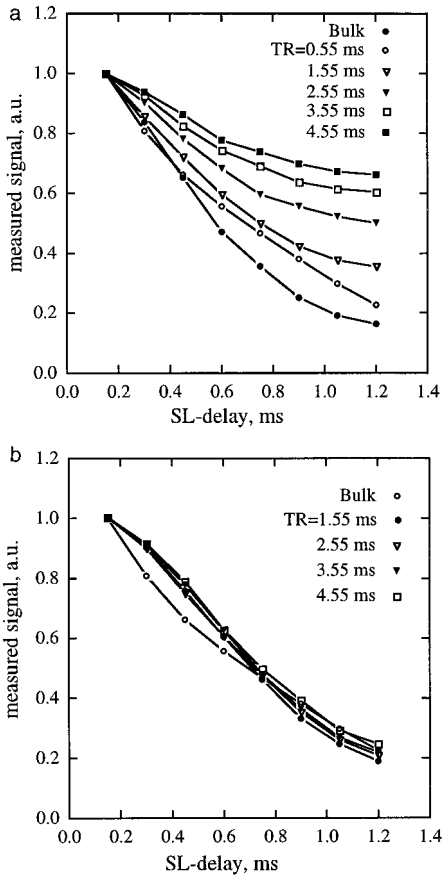

FIG. 7. Measurements of $T_{1\rho}$ for SL fields of 0.1 G which correspond to a $T_{1\rho}$ of 0.72 ± 6 ms. Various repetition times TR are employed. (a) Measurements by full-ramp SPRITE. The values derived from the SPRITE images differ from the bulk measurements. (b) Measurements by half-ramp SPRITE. There is no significant difference in measurements with various TR values and they agree with the bulk measurements.

Note that while for a full ramp *k*-space acquisition with phase encoding, only relative phase changes are significant, for a half *k*-space acquisition with reconstruction of the missing data prior to Fourier transformation, absolute phase values are important. Therefore, after conjugation, if for some reason the spectrometer frequency is misadjusted, one must multiply the conjugated data by a phase difference; otherwise, phase distortions will appear in the image.

EXPERIMENTAL

The SPRITE technique was implemented on a Nalorac (Martinez, CA) 2.4 T 32 cm i.d. horizontal bore superconducting magnet. A water cooled 7.5 cm i.d. gradient set (maximum gradient strength 100 G cm^{-1}) was employed, driven by Techron (Elkhart, IN) 7780 amplifiers. The RF probe was a homebuilt 32 strut bird-cage coil. It was driven by a 2 kW AMT (Brea, CA) 3445 RF amplifier. All experiments were performed at ambient temperature with a Tecmag (Houston, TX) Libra S-16 console.

Our philosophy for magnetization preparation follows closely that of Bluemler and Bluemich (*10*) with the difference that our preparation always involves *Z*-magnetization, usually with *Z*-storage for each line of *k*-space (Fig. 5).

In our spin lock (SL) preparation experiments, the maximum SL magnetic field was 2.2 G. Our spin lock phantom was a block of polyisoprene (Aldrich) with relaxation parameters as follows: $T_1 = 145 \pm 2$ ms, $T_2^* = 1.1$ ms. Spin-locking was applied in the conventional way (*30*), that is, after a $(90)_x$ excitation pulse, a *y*-pulse was applied for fixed delay to lock spins in the *Y*-direction of the rotating frame. Measurements with various SL-delays and SL-field strengths were performed. SL-delays were changed from 0.2 to 1.6 ms in steps of 0.4 ms. After SL-evolution, a $(90)_{-x}$ pulse was used for *Z*-storage, to conserve the SL-prepared magnetization as longer lifetime longitudinal magnetization. For bulk measurements a $(90)_x$ pulse was used to generate an FID. Bulk $T_{1\rho}$- measurements are incorporated with imaging measurements in Fig. 5. SPRITE acquisitions with both centric and sequential order encoding were performed. The phase-encoding time t_p was 100 μs and maximum phase-encoding gradients were 12 G cm^{-1}. 1D-64-points profiles were acquired with a nominal resolution of 0.88 mm/pixel. Several TR times were used: 0.55, 1.55, 2.55, 3.55, and 4.55 ms. These corresponded to 35, 99, 163, 227 and 291 ms acquisition times for sequential SPRITE with 64 acquisition points and 17.6, 25, 81.6, 113.6 and 145.6 ms for half *k*-space centric order SPRITE. Because the T_2^* of polyisoprene is long, 1.1 ms, compared to the shortest TR, 0.55 ms, active gradient spoiling (2 G/cm during 0.3 ms) was after the single point acquisition at each gradient level.

For inversion-recovery (IR) measurements, a cylindrical sample, 4 cm diameter, 6 cm height, consisting of polyethylene shell and PVC core was employed. The T_1 of polyethylene was biexponential, corresponding to amorphous and semicrystalline components of 360 ± 8 ms and 11 ± 1 ms, respectively. The T_2^* was 320 ± 9 μs. The T_1 of PVC was essentially single-exponential, 144 ± 6 ms with a T_2^* of 362 ± 8 μs. For IR-nulling, a 180-pulse was applied with a delay τ before data acquisition. The delay corresponded to the null point of the inversion recovery of longitudinal PVC-magnetization ($\tau = T_1 \ln 2 = 100$ ms). The imaging parameters were as follows: t_p was 75 μs and maximum phase-encoding gradients were 12 G cm^{-1} in both directions, $FOV_x = FOV_y = 7.5$ cm, with 64 × 64 pixels. The number of SPRITE half-ramp points *N* was 64/2, with a nominal resolution of 1.2 mm. The TR was 0.45 ms with a T_d for magnetization recovery of 0.9 s. The number of averages was 4, giving a total imaging time of 3 min 50 s.

The resolution phantom was a disk of crosslinked *cis*-polybutadiene, 4 cm diameter and 0.8 cm thickness, with relaxation parameters $T_1 = 221 \pm 9$ ms, $T_2^* = 336 \pm 12$ μs. The

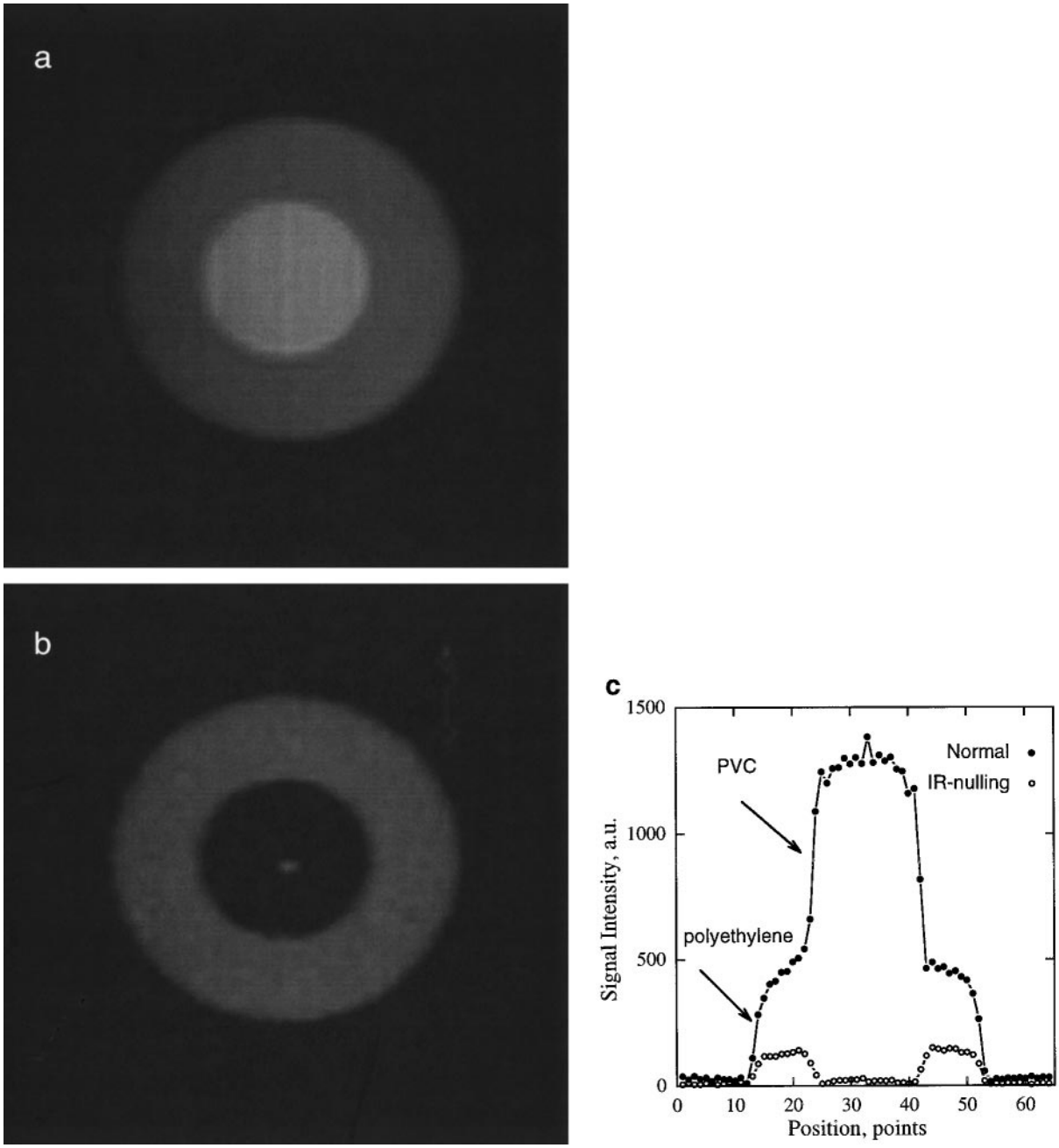

FIG. 8. (a) Half-SPRITE image of a composite cylinder with a PVC core and polyethylene shell without IR nulling. The PVC signal dominates the image. (b) Half-SPRITE image of the same sample with IR nulling (the delay, T_{1PVC} ln 2, is 99 ms). No PVC signal is observed. (c) Cross-sections of the two images at the same scale. One can see that the PVC signal is totally removed by IR nulling while the polyethylene signal has a decreased intensity. Pixel size is 1.2 mm.

imaging parameters were as follows: encoding time $t_p = 100$ μs, gradient strength $G_x = G_y = 12$ G/cm, $FOV_x = FOV_y = 5.6$ cm, 64×64 pixels, with the number of SPRITE ramp points $N = 64$ (32 for half k-space sampling). The nominal resolution was 0.88 mm. The SPSF resolution was 1.21×0.88 mm = 1.06 mm, $TR/T_1 = 0.01$, with a T_d 1.1 s for magnetization recovery. Eight averages were acquired for a total imaging time of 9 min 20 s.

RESULTS AND DISCUSSION

In our original SPRITE paper (*5*) transient state effects were noted in the contrast of samples with T_1-relaxation times on the order of the duration of the primary phase encode ramp. In the Theory section we have provided a theoretical explanation of transient longitudinal magnetization effects in SPRITE imaging and explained how transient effects should influence pre-

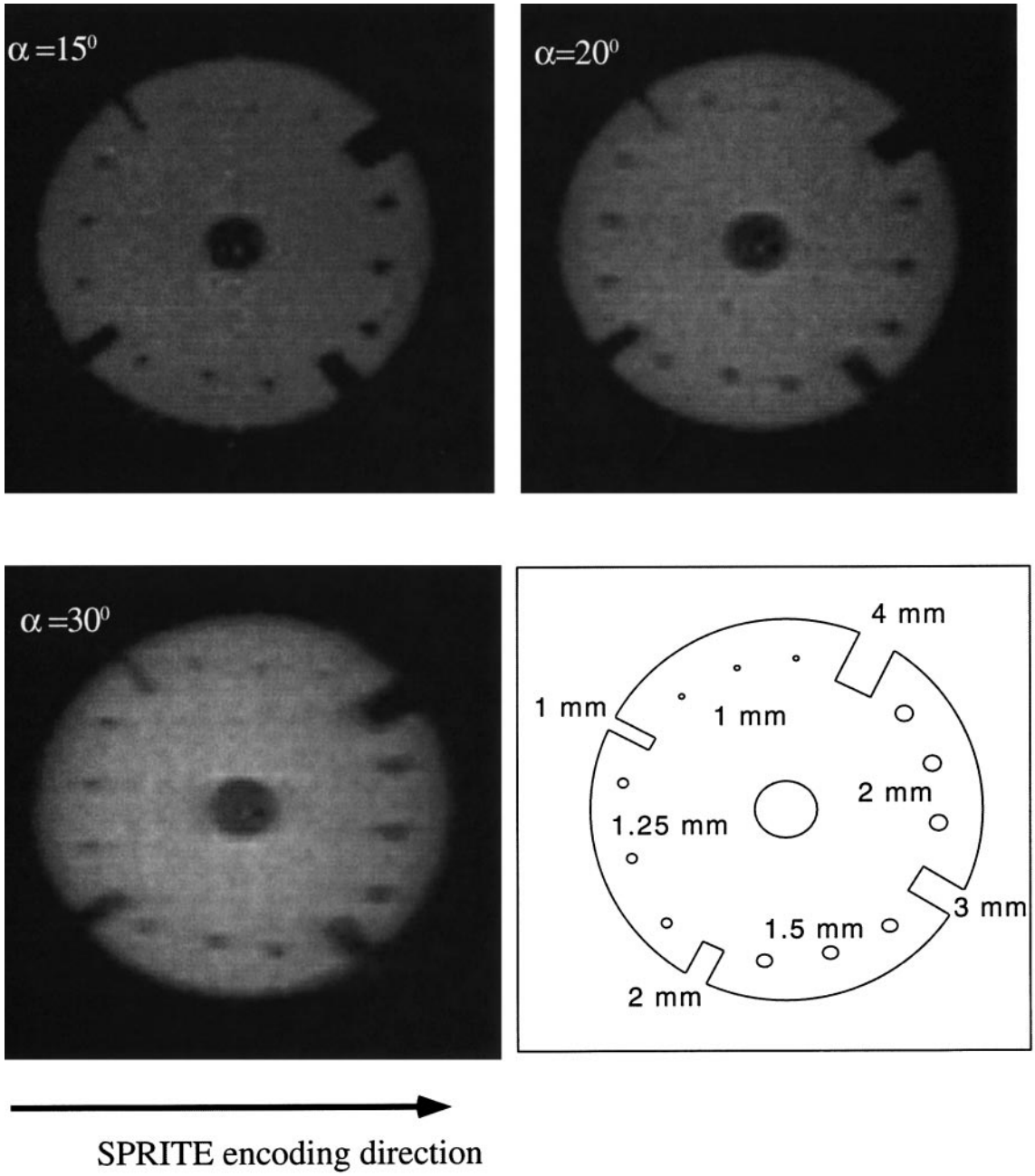

FIG. 9. Half-ramp SPRITE images of a resolution phantom made from crosslinked polybutadiene. The pulse flip angles were 15°, 20°, and 30° (clockwise from top left); the same dynamic scale is used for image presentation. Both signal-to-noise and resolution blurring increase as flip angle increases. The bottom right panel shows a schematic of the phantom with characteristic sizes of the voids indicated.

pared magnetization and image resolution. A variety of half *k*-space centric and full *k*-space sequential sampling SPRITE images of realistic materials were acquired to validate the advantages of SPRITE for solid-like materials.

SPRITE imaging of solid-like materials, with prepared magnetization, is conceptually similar to liquid-state snapshot FLASH imaging (*31*). Magnetization-prepared FLASH permits acquisition of an entire line of *k*-space for each excitation pulse and, in principle, 2D *k*-space for each magnetization preparation. SPI-based methods, however, permit only one point of *k*-space to be acquired for each excitation pulse and, consequently, one line of *k*-space for each magnetization preparation. Although the SPRITE technique permits shorter TR times than SPI, there are still restrictions on the overall image acquisition time due to gradient rise times, as well as gradient coil and amplifier duty cycles. Our imaging system requires at least 200 μs per gradient step for gradient stabilization. To acquire one half-line of *k*-space therefore requires at least 6.4

ms for a 64-point line. This restricts the applicability of the technique to materials with T_1 no shorter than 10 ms. For even shorter T_1's one could return to a simple SPI sequence with rapidly switched gradients and apply a spin preparation for each k-space point.

Theory shows that magnetization evolution during sampling will be most severe for samples with their initial magnetization substantially altered from the equilibrium value. Therefore, in spin-lock magnetization preparation test experiments a weak spin lock field (0.1 G) was chosen for our sample where $T_{1\rho}$ was already short (0.72 $\pm$ 6 ms) (Fig. 6). For this $T_{1\rho}$, the Z stored magnetization after the longest spin lock delay (1.2 ms) was less than 20% of the equilibrium magnetization. Bulk and image derived $T_{1\rho}$ results are displayed in Fig. 7 for (a) sequential order and (b) half k-space centric order encoding. For the centric order encoding experiments the observed $T_{1\rho}$ values coincide with the bulk measurement for all TRs while they systematically diverge from the bulk value with sequential order encoding at long TRs.

Nulling chosen T_1 populations through an inversion recovery (IR) preparation is an attractive modification of the SPRITE experiment that will greatly increase image contrast. It is also a preparation technique, which is anticipated to have the greatest transient effects on the image resolution. Images of a cylindrical PVC, polyethylene composite phantom are shown in Fig. 8. One image (Fig. 8b) shows that the PVC polymer signal from the phantom is easily nulled by the choice of an appropriate delay after an inversion pulse with half k-space centric encoding. The other image (Fig. 8a) is a control with no inversion recovery magnetization preparation. The PVC signal in Fig. 8a is much greater than of polyethylene; however, it is completely suppressed after IR nulling in Fig. 8b. Cross-sections through the image centers are displayed in Fig. 8c. The detailed contrast and resolution features of the general IR nulling experiment will be the subject of a separate communication.

As with all SPI type experiments, one must consider the pulse bandwidth when comparing the results of images acquired with different flip angles. In this work the typical 180°-pulse length was 55 μs. For maximum gradients of 12 G cm^{-1} the required excitation band was $\gamma G_{\max} L/2 = 100$ kHz, where L again is the characteristic size of a sample. The longest RF-pulse homogeneously irradiating the sample was therefore approximately 10 μs. This corresponds to a flip angle of 33°. The upper limit to the pulse flip angle in this work was therefore fixed at 30°.

To examine pulse flip angle effects on image intensity and resolution, a series of experiments, centric encoding, were undertaken with a crosslinked polybutadiene phantom. Figure 9 shows representative two-dimensional images of the phantom acquired with 15, 20, and 30° flip angles. The images are displayed with a common gray scale. According to Eq. [4], with the imaging and sample parameters chosen, resolution will be degraded once the flip angle exceeds 20 degrees. Note

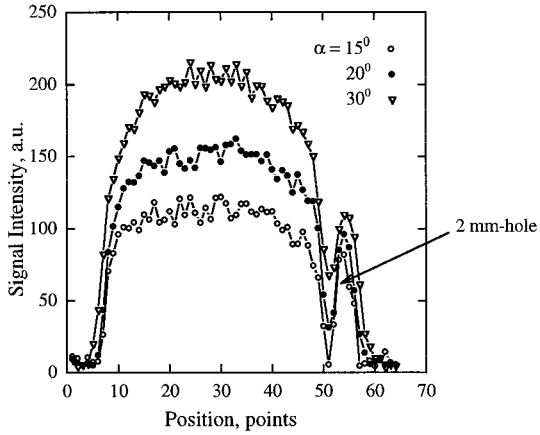

FIG. 10. Cross-sections of the resolution phantom images of Fig. 9 through a 2-mm hole. Note that resolution decreases as the flip angle increases. The pixel size is 0.88 mm.

that blurring increases with flip angle, in the direction of the primary phase encode gradient. For a more detailed analysis, cross-sections in the SPRITE direction of the images are displayed in Fig. 10. The cross-section goes through a 2-mm hole in the phantom and it is seen that resolution decreases as the flip angle increases. The overall shape of the profiles is identical, which means that irradiation of the sample is homogeneous and blurring can be ascribed to transient state effects alone. (Any visual differences are due to differences in signal amplitudes; after normalization the shapes are the same).

To estimate the S/N improvement with centric encoding, phantom images with a half k-space acquisition (imaging parameters as above, flip angle = 15°) and a full k-space acquisition (imaging parameters as above, but flip angle = 8°) were compared. Profiles through the center of the sample are shown in Fig. 11. The experimental S/N ratio of the two images was 2.5, in favor of the centric half k-space image. The predicted value was 2.6. The increased S/N could be used to decrease the number of averages by a factor of $(2.6)^2 \sim 6$–7 to attain the same S/N as for conventional SPRITE imaging. If one combines the half k-space acquisition with delays T_d of less than 5 T_1, it yields a reduction in the acquisition time for imaging of solid-like materials with magnetization preparation techniques of greater than a factor of 10 in comparison to conventional magnetization-prepared SPRITE.

CONCLUSION

We have demonstrated in this work that centric order encoding applied to a SPRITE acquisition significantly increases the S/N while permitting the use of any magnetization preparation technique without degrading, within bounds, image resolution. For materials with short T_2^*, transverse magnetization is easily spoiled, and this allows us to estimate the transient-state longitudinal magnetization behavior and its influence on

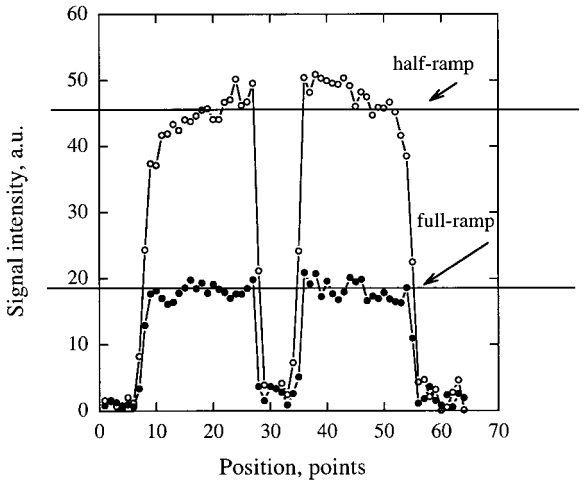

FIG. 11. Cross-section through half-ramp SPRITE (flip angle = 15°) and full-ramp SPRITE (flip angle = 8°) images. The signal of the former is 2.5 times higher than of the latter. The predicted value was 2.6 (3.7/1.4). The factor of 3.7 is an increase due to centric order encoding, while the 1.4 factor is a decrease due to limited data in the half *k*-space acquisition. Pixel size is 0.88 mm.

spatial resolution. One is able therefore to rationally trade resolution for increased S/N as desired.

A half *k*-space acquisition for SPI-based methods is achieved with minimal phase correction. The increased S/N permits a reduced number of signal averages, and hence a total acquisition time decrease of a factor of 10 when compared to conventional SPRITE with prepared magnetization. If signal averaging is not required, the centric half *k*-space acquisition gives a noticeable increase in S/N with a decreased acquisition time.

One very practical advantage of the half *k*-space centric encoding strategy with SPRITE is that it removes T_1 as a factor in the image intensity. It is introduced instead as a factor controlling image resolution.

ACKNOWLEDGMENTS

We thank NSERC of Canada for a NATO Science Fellowship (IVM) and operating and equipment grants (BJB). We also thank Albert R. Cross and Rod MacGregor for their technical assistance and Don Hornibrook for the fabrication of the imaging phantoms.

REFERENCES

1. S. Emid and J. H. N. Creyghton, *Physica B* **128,** 81 (1985).
2. D. E. Axelson, A. Kantzas, and T. Eads, *Can. J. Appl. Spectrosc.* **40,** 16 (1995).
3. S. Gravina and D. G. Cory, *J. Magn. Reson. B* **104,** 53 (1994).
4. J. C. Sharp, R. W. Bowtell, and P. Mansfield, *Magn. Reson. Med.* **29,** 407 (1993).
5. B. J. Balcom, R. P. MacGregor, S. D. Beyea, D. P. Green, R. L. Armstrong, and T. W. Bremner, *J. Magn. Reson. A* **123,** 131 (1996).
6. S. D. Beyea, B. J. Balcom, P. J. Prado, A. R. Cross, C. B. Kennedy, R. L. Armstrong, and T. W. Bremner, *J. Magn. Reson.* **135,** 156 (1998).
7. P. J. Prado, B. J. Balcom, S. D. Beyea, R. L. Armstrong, and T. W. Bremner, *Solid State NMR* **10,** 1 (1998).
8. C. B. Kennedy, B. J. Balcom, and I. V. Mastikhin, *Can. J. Chem.,* in press (1998).
9. P. T. Callaghan, "Principles of Nuclear Magnetic Microscopy," Clarendon Press, Oxford (1993).
10. P. Bluemler, and B. Bluemich, *Magn. Reson. Imaging* **10,** 779 (1992).
11. M. T. Vlaadingerbroek and J. A. den Boer, "Magnetic Resonance Imaging," Springer-Verlag, Berlin (1996).
12. J. Frahm, W. Hanicke, and K. D. Merboldt, *J. Magn. Reson.* **72,** 307 (1987).
13. W. Hanicke, K. D. Merboldt, D. Chien, M. L. Gyngell, H. Bruhn, and J. Frahm, *Med. Phys.* **17,** 1004 (1990).
14. E. M. Haacke, *Magn. Reson. Med.* **4,** 407 (1987).
15. S. Braun, H.-O. Kalinowski, and S. Berger, "100 and More Basic NMR Experiments," VCH, Weinheim (1996).
16. A. Holsinger and S. J. Riederer, *Magn. Reson. Med.* **16,** 481 (1990).
17. J. Hennig, *Concepts Magn. Reson.* **3,** 125 (1991).
18. M. K. Stehling, *Magn. Reson. Imaging* **10,** 165 (1992).
19. D. Chien, D. J. Atkinson, and R. R. Edelman, *J. Magn. Reson. Imaging* **1,** 63 (1991).
20. H. Lee and R. R. Price, *J. Magn. Reson. Imaging* **4,** 837 (1994).
21. G. Johnson, D. Feinberg, and V. Venkataraman, *J. Magn. Reson. Imaging* **6,** 944 (1996).
22. A. H. Wilman and S. J. Riederer, *Magn. Reson. Med.* **36,** 384 (1996).
23. A. H. Wilman and S. J. Riederer, *Magn. Reson. Med.* **38,** 793 (1997).
24. J. P. Mugler III, F. H. Epstein, and J. R. Brookeman, *Magn. Reson. Med.* **28,** 165 (1992).
25. F. H. Epstein, J. P. Mugler III, and J. R. Brookeman, *J. Magn. Reson. Imaging* **4,** 91 (1994).
26. D. Feinberg, J. Hale, J. Watts, L. Kaufman, and A. Mark, *Radiology* **161,** 527 (1986).
27. P. Margosian, F. Schmitt, and D. E. Purdy, *Health Care Instrum.* **1,** 195 (1986).
28. E. M. Haacke, E. D. Lindskog, and W. Lin, *J. Magn. Reson.* **92,** 126 (1991).
29. G. McGibney, M. R. Smith, S. T. Nichols, and A. Crawley, *Magn. Reson. Med.* **30,** 51 (1993).
30. R. Kimmich, "NMR Tomography, Diffusometry, Relaxometry," Springer-Verlag, Berlin (1997).
31. A. Haase, *Magn. Reson. Med.* **13,** 77 (1990).